Structure of Antibody-Bound Peptides and Retro−Inverso Analogues. A Transferred Nuclear Overhauser Effect Spectroscopy and Molecular Dynamics Approach[†,‡]

Angélique Phan-Chan-Du,[§] Marie-Christine Petit,[§] Gilles Guichard,[||] Jean-Paul Briand,[||] Sylviane Muller,[||] and Manh Thong Cung*[,§]

Laboratoire de Chimie-Physique Macromoléculaire, UMR 7568 CNRS-INPL, Groupe ENSIC, 1 rue Grandville, B.P. 451, 54001 Nancy Cedex, France, and Institut de Biologie Moléculaire et Cellulaire, UPR 9021 CNRS, 67000 Strasbourg, France

Received May 22, 2000; Revised Manuscript Received January 23, 2001

ABSTRACT: The three-dimensional structures of the two L-peptides, H-CGGIRGERA-OH, called L(A), and H-CGGIRGERG-OH, called L(G), corresponding or close to the IRGERA sequence present in the C-terminal region (residues 130−135) of histone H3, and their retro−inverso analogues HO-mAreGriGGC-NH_2, called RI(mA), and HO-mGreGriGGC-NH_2, called RI(mG), have been studied by two-dimensional ^{1}H NMR and molecular dynamics calculations in association with a monoclonal antibody generated against L(A). At 25 °C, the affinity constants of the monoclonal antibody with respect to RI(mA) and RI(mG) were 75- and 270-fold higher than those measured with the homologous L(A) and L(G) peptides, respectively. Due to the spontaneous epimerization of the mA malonic residue, RI(mA) gave rise to two sets of resonances. With regard to the NH amide region, one set was similar to that for RI(mG) while the second was similar to those for the parent L-peptides L(A) and L(G). The antibody-bound conformations of the two couples of L- and retro−inverso peptides have been analyzed using molecular modeling calculations based on the transferred NOE interproton distances. Folded structures appeared in both cases with a type II′ β-turn in the parent GGIR sequence and a type I′ β-turn in the retro−inverso reGr sequence.

A serious limitation to the use of peptides for therapeutic applications lies in their weak resistance to biodegradation. They are usually short-lived molecules which are rapidly degraded in vivo by proteases. It has been known for many years that the introduction of backbone modifications into peptides can affect the potency, enzymatic stability, and conformational properties of the resulting analogues. In some cases, this strategy led to the production of analogues with advantageous biological and functional properties. The generation of structural mimics related to neuropeptides, peptide hormones, peptide antibiotics, or more recently peptides with potential use in vaccination has thus attracted considerable attention (*1*−*4*). The modifications introduced into peptides are for example the replacement of L-amino acid by D-amino acid residues or by unnatural ones and/or the modification of peptide bonds. Peptidomimetics containing reduced peptide bonds $\psi(CH_2-NH)$ and retro−inverso modifications $\psi(NH-CO)$ instead of the natural peptide bond $\psi(CO-NH)$ have been particularly investigated, at both the structural and biological levels (*5*−*11*).

The recent finding that retro−inverso analogues, also known as all-D retro or retro−enantio peptides, can present equivalent or superior antigenic and immunogenic properties compared with those of the corresponding parent peptides is very promising and has many potential applications in the development of synthetic vaccines and new strategies in immunomodulation. We have previously studied the immune cross reaction between parent L-peptides and their corresponding all-D retro peptide analogues in different antigenic systems, namely, the IRGERA hexapeptide corresponding to C-terminal residues 130−135 in histone H3 (*12*, *13*) and the major antigenic site of the foot-and-mouth disease virus (FMDV)[1] VP1 protein (*14*−*16*). The use of totally or partially retro−inverso peptides as antigenic targets for autoantibodies in replacement of natural peptides or as ligands to immune system receptors has also been found to be very useful (*17*−*20*). It was shown, for example, that a single inoculation of the FMDV peptide 141−159 in the retro−inverso form elicited neutralizing and protective antibodies

† This work was supported in part by a grant from Centre National de la Recherche Scientifique ("Physique et Chimie du Vivant" programme).

‡ The atomic coordinates of the parent and retro−inverso peptide structures reported in this paper have been deposited in the Protein Data Bank (Brookhaven National Laboratory, Upton, NY) as entries 1cs9, 1ct6, 1cvq, 1cw8, and 1cwz, respectively.

* To whom correspondence should be addressed: Laboratoire de Chimie-Physique Macromoléculaire, UMR 7568 CNRS-INPL, Groupe ENSIC, 1 rue Grandville, B.P. 451, 54001 Nancy Cedex, France. Phone: (33) 3 83 17 51 07. Fax: (33) 3 83 37 99 77. E-mail: Manh-Thong.Cung@ensic.inpl-nancy.fr.

§ UMR 7568 CNRS-INPL.

|| UPR 9021 CNRS.

[1] Abbreviations: BSA, bovine serum albumin; DG, distance geometry calculations; EDC, *N*-ethyl-*N*′-[3-(dimethylamino)propyl]carbodiimide; ELISA, enzyme-linked immunosorbent assay; EM, energy minimization; FMDV, foot-and-mouth disease virus; HPLC, high-performance liquid chromatography; MD, molecular dynamics; mA, malonic analogue of alanine [stands for CO-CH(CH_3)-CO]; mAb, monoclonal antibody; mG, malonic analogue of glycine (stands for CO-CH_2-CO); NOESY, nuclear Overhauser enhancement spectroscopy; PDEA, 2-(2-pyridinyldithio)ethane amine; RI, retro−inverso; rmsd, root-mean-square deviation; SA, dynamical simulated annealing; TMPS-d_4, 2,2,3,3-tetradeuterio(trimethylsilyl)-3-propionic acid sodium salt; TPPI, time-proportional phase incrementation; TOCSY, total correlation spectroscopy; TR-NOE, transferred nuclear Overhauser enhancement; VP1, viral capsid protein 1; WATERGATE, water suppression by gradient-tailored excitation.

10.1021/bi001151h CCC: $20.00
Published on Web 04/19/2001

in guinea pigs and pigs (*15*, *16*). An NMR analysis in aqueous solution showed that the retro−inverso peptide analogue was more rigid than the parent L-peptide (*21*). The higher affinity of the retro−inverso peptide 141−159 for the antivirus, antiprotein, or antipeptide antibodies probably has to be related to these structural features (*14*, *15*).

We have previously established that the equilibrium affinity constant K_a for the IRGERA retro−inverso analogue to various monoclonal antibodies generated against the parent peptide was 7−75-fold higher than that for the homologous L-peptide (*13*). Understanding the fine mechanisms of this antibody−antigen interaction is important in the effort to design synthetic antigens presenting an improved antibody affinity. In the study presented here, we have carried out two-dimensional transferred nuclear Overhauser enhancement experiments (TR-NOESY) (*22*) and molecular dynamics simulation to determine the structural properties of the two L-peptides, H-CGGIRGERA-OH, called L(A), and H-CGGIRGERG-OH, called L(G), and the two corresponding retro−inverso analogues, HO-mAreGriGGC-NH_2, called RI(mA), and HO-mAreGriGGC-NH_2, called RI(mG), when bound to a monoclonal antibody directed against L(A). To our knowledge, only five two-dimensional NMR structural studies of peptides and their retro−inverso analogues have been reported so far, but only concern free peptides in polar, aqueous, or micellar environment (*21*, *23*−*26*). The TR-NOESY experiment has been used to determine the conformations of a wide range of small ligands in the protein-bound state by focusing on the easily detected NMR signals of the free ligands (*27*−*30*).

MATERIALS AND METHODS

Peptides. The sequence CGG, acting as a spacer, was added to the N-terminus of the IRGERA sequence. The Cys thiol group served as a linker to (i) the dextran matrix in BIAcore experiments (see below) and (ii) the carrier protein, bovine serum albumin (BSA), after treatment with *N*-succinimidyl 3-(2-pyridyldithio)propionate. The peptides and their retro−inverso analogues were synthesized by the stepwise solid-phase methodology on a multichannel synthesizer (*31*) using the *tert*-butyloxycarbonyl (Boc) or 9-fluorenylmethyleneoxycarbonyl (Fmoc) chemistry (*13*). Boc- and Fmoc-protected L- and D-amino acid derivatives were purchased from Neosystem (Strasbourg, France). The (*R*,*S*)-2-methylmalonic acid monobenzyl ester, obtained by alcoholysis of 2,2,5-trimethyl-1,3-dioxane-4,6-dione (*32*), reacted with the preformed peptide chain as a racemate. After acid cleavage from the resin, the different peptides were purified by reversed-phase middle-pressure liquid chromatography, but the two RI(mA) diastereomers could not be separated. The final purity was greater than 90% as checked by analytical HPLC. The peptide identity was verified by matrix-assisted laser desorption/ionization mass spectrometry (MALDI-MS) using a protein TOF apparatus (Bruker, Wissembourg, France) and gave the expected results for all peptides (data not shown). To gain clarity, L-residues are represented by their one-letter uppercase abbreviations while one-letter lowercase abbreviations are used for D-residues. Residues are numbered in the direction of the peptide CO−NH bond.

Monoclonal Antipeptide Antibody and Kinetic Analysis of mAb Binding. As previously described, the mAb 4x11 monoclonal antibody (IgG1), abbreviated as mAb, was generated from BALB/c mice immunized against the liposome-coupled peptide L(A) (*13*). It was selected because of the wide variation of its apparent affinity constant K_a, which was determined using the BIAcore biosensor system (BIAcore AB, Uppsala, Sweden) (*13*), to the different antigenic peptides and their retro−inverso analogues. The standard procedure was used for immobilizing the cysteine-containing peptides on the sensor chip (*13*). The carboxyl−dextran matrix was first activated with 0.2 M *N*-ethyl-*N*′-[3-(dimethylamino)propyl]carbodiimide (EDC) and 0.05 M *N*-hydroxysuccinimide. It was further modified by injecting 2-(2-pyridinyldithio)ethane amine (PDEA) thiol coupling reagent [15 μL of 80 mM PDEA in 0.1 M borate buffer (pH 8.5)], allowing the thiol reactive group of peptide analogues to be coupled to the activated matrix. After the peptide immobilization run, the remaining reactive groups on the sensor surface were deactivated by a 4 min pulse of 50 mM cysteine in 1 M NaCl (pH 4.3). Measurement of affinity constants was performed as described previously (*33*). The ELISA procedure was as described previously (*34*).

NMR Experiments. The optimal conditions for the TR-NOESY measurements were determined by considering an L(A)/mAb molar ratio from 10 to 100 with four mixing times (τ_m) ranging from 100 to 500 ms. The buildup curve (*35*) for different NOE correlations showed that spin diffusion was negligible for a τ_m of 200 ms. The peptide/mAb molar ratio was adjusted to 50/1 (i.e., 5 mM peptide and 0.1 mM mAb) in H_2O and D_2O (95/5, v/v) at pH 7.0 (100 mM phosphate buffer containing 0.02% sodium azide). These conditions led to intense, negative transferred NOESY cross-peaks assigned to the mAb-bound antigen (*36*). ^{1}H NMR spectra were recorded on a Bruker DRX-400 spectrometer at 4 °C with TMPS-d_4 as an internal reference. The two-dimensional TOCSY and NOESY data were acquired in the pure-phase absorption mode with quadrature detection in both dimensions using the States−TPPI mode. The two-dimensional data sets were collected with a 5000 Hz spectral width using 2048 data points in the F_2 dimension and 512 experiments in the F_1 dimension. The carrier frequency was set on the residual water signal. In all experiments, water resonance was selectively suppressed by using the WATERGATE sequence (*37*). The intensity of peaks was extracted from the NOESY spectra (τ_m = 200 ms) using XEASY software (*38*), and the interproton distances were calculated taking the distance of 1.78 Å between the two Cys-C$^\beta$H$_2$ protons as a reference. Distance restraints were assigned as strong, medium, and weak and set as intervals of 1.8−2.5, 2.5−3.5, and 3.5−5.5 Å.

Molecular Dynamics Calculations. Energy minimization (EM) and molecular dynamics (MD) calculations were performed on an Indy Silicon Graphics workstation using DYANA-1.4 (*39*) and DISCOVER (Molecular Simulations Inc., San Diego, CA) and the consistent-valence force field CVFF (*40*). A distance-dependent dielectric constant equal to 4*r* was applied with a 16 Å cutoff radius to evaluate electrostatic interactions. To impair the structural artifacts due to overestimation of Coulomb interactions in vacuo, the net electric charges of the ionic Arg and Glu residues were decreased to half of their initial value, while those of the N- and C-terminal charged groups were neglected. For each derivative, a variable set of 35−60 backbone−backbone,

backbone−side chain, and side chain−side chain distance restraints was implemented in the calculations with a force constant scaled to 20 kcal mol^{-1} Å^{-2}. The ϕ angle for the non-glycine L-residues was constrained between −175° and 0°, and inversely between 0° and 175° in the case of the D-residues. On the basis of the NOE connectivities which are specific for a β-turn sequence (*41*), we have introduced the R5 NH−G2 CO hydrogen bond for the L-peptides and the r5 NH−r2 CO hydrogen bond for the retro−inverso peptides by constraining the H···O distance between 1.5 and 2.4 Å with a force constant scaled to 10 kcal mol^{-1} Å^{-2} at the beginning of MD simulations and reduced to 2 kcal mol^{-1} Å^{-2} at the end of the calculations. As all the main chain atoms have a *z*-coordinate equal to zero in the DYANA-1.4 residue library (*39*), the D-amino acids were introduced by changing only the sign of the non-zero *z*-coordinate (H^{α} and side chain atoms). The malonic acid residues were also introduced into the library from the Gly or Ala residue which was modified using MOLMOL-2.5.1 software (*42*). Two simulation runs were performed on the RI(mA) retro−inverso peptide containing either the (*R*)- or (*S*)-2-methylmalonic residue.

Structure calculations were performed using a simulated annealing (SA) protocol which involved the exploration of the maximum conformational space in determining the global minimum energy conformation of the molecule. SA has been shown to be a useful procedure for the study of constrained systems (*43*−*45*). Starting from the extended structure, we performed the SA calculations according to a protocol adapted from Nilges et al. (*43*), and the calculations consisted of the following stages: (i) an initial EM of randomly distributed atoms (300 steps of steepest descent, 300 steps of conjugate gradient, and 300 steps of the Newton−Raphson method), (ii) 200 ps of restrained molecular dynamics at 1000 K with structure saving every 4000 iterations for 1.0 fs in each step so that a total of 50 structures were generated, and (iii) 5 ps of restrained molecular dynamics applied to each structure during cooling from 1000 to 300 K in eight stages, followed by a final EM stage (300 steps of steepest descent, 300 steps of conjugate gradient, and 300 steps of the Newton−Raphson method).

RESULTS

mAb Affinity. The reactivity of mAb generated against L(A) was measured in a direct ELISA format in which BSA-conjugated peptides were used for coating plates. In this ELISA format, mAb reacted equally well with both L(A) and RI(mA) peptides (OD values measured at 450 nm were 1.29 and 1.12, respectively) (*13*, *34*). We determined the kinetic rate and equilibrium affinity constants of the mAb for the different peptides which were immobilized on the chip. The K_a equilibrium affinity constant values for L(A) and L(G) were very similar, i.e., 3×10^6 and 7×10^6 M^{-1}, respectively. It is noteworthy that the analogue H-CGGIR-GERa-OH, called L(a), only differing from L(A) in the chirality of the C-terminal alanine, was not recognized by the mAb. The latter bound more strongly to the two retro−inverso analogues, with 75- and 270-fold higher K_a values for RI(mA) and RI(mG) than for the L(A) and L(G) peptides, respectively. We noted that the highest K_a affinity constant was obtained with RI(mG), 1.9×10^9 M^{-1}, and approached the K_a value measured for the cognate protein histone H3, 2.3×10^9 M^{-1} (*13*). As RI(mA) is a mixture of two diastereomers, the affinity constant is probably an average value which may indicate that one of the diastereomers binds with higher affinity to mAb than the other one.

^{1}H NMR Analysis. The absence of negative NOEs for the free ligand reflects both the small size of the ligand and the short correlation time. Only a few and weak negative NOEs were observed for the 10/1 peptide/mAb molar ratio. Their number and intensity increased with the peptide/mAb molar ratio up to a value of 75/1 and then decreased for a value of 100/1. Moreover, only one set of NH resonances, with chemical shifts corresponding to the free ligand, was observed for all of the peptide/mAb ratios, even for the lowest value (10/1). These combined results show that the chemical exchange rate is fast compared to the cross-relaxation rate and should correspond to a dissociation constant K_D exceeding 10^{-5} M. Actually, TR-NOEs are very weak for K_D values of $<10^{-6}$ M, and are smaller than those for the free ligand in the case of intermediate K_D values between 10^{-5} and 10^{-6} M. This observation denotes that the NOE is transferred from the bound state to the free ligand via chemical exchange in agreement with the theoretical evaluation of the two-dimensional TR-NOESY spectra proposed by Campbell and Sykes in which the effects of different variables such as mixing time, fraction of bound ligand, correlation time, internal motion in the free and bound ligand, and other contributions to spin−lattice relaxation rates were examined (*46*, *47*). For a protein with a molecular mass of 80 kDa, simulation predicted a fast buildup of near 5% of the bound peptide followed by a rapid decay when the fraction of bound peptide decreases. The interval of fraction of bound peptide, for which the buildup of TR-NOEs and their maximum values should be observed, becomes more and more narrow when the size of the protein increases. Thus, the larger the protein is, the smaller the amount of bound ligand required to achieve an intense TR-NOE is. For a very high peptide/mAb ratio, the residence time of the ligand in contact with the protein decreases till a certain threshold where it is too short for building up the TR-NOE. In the theoretical evaluation of the effects due to internal motions on the buildup of the two-dimensional TR-NOE, Campbell and Sykes have pointed out that the internal motions in the free peptide contribute more to the overall relaxation of the exchanging system than do motions in the bound peptide, a consideration which may be overlooked given the fact that it is the faster cross relaxation in the bound peptide that determines the buildup rates of the TR-NOE (*47*).

The proton resonances have been assigned by a combination of COSY, TOCSY, and NOESY experiments according to established methods (*48*), and the multiple Gly and Arg residues have been sequenced on the basis of the NN(i,i+1) and αN(i,i+1) NOE connectivities. Probably because of fast proton exchange with water, the G2 broad amide signal was not identified for both L-peptides. As expected, the NMR spectrum for RI(mG) presents a single set of spin systems. Due to the mixture of two diastereomers, the NMR spectrum of RI(mA) is rather complicated with two sets of overlapping spin systems (Figure 1). One set is closely similar to that for RI(mG), and is assigned to the diastereomer that we call RIa(mA). The second diastereomer is named RIb(mA).

The conformational differences between the parent peptides and the retro−inverso analogues can be qualitatively

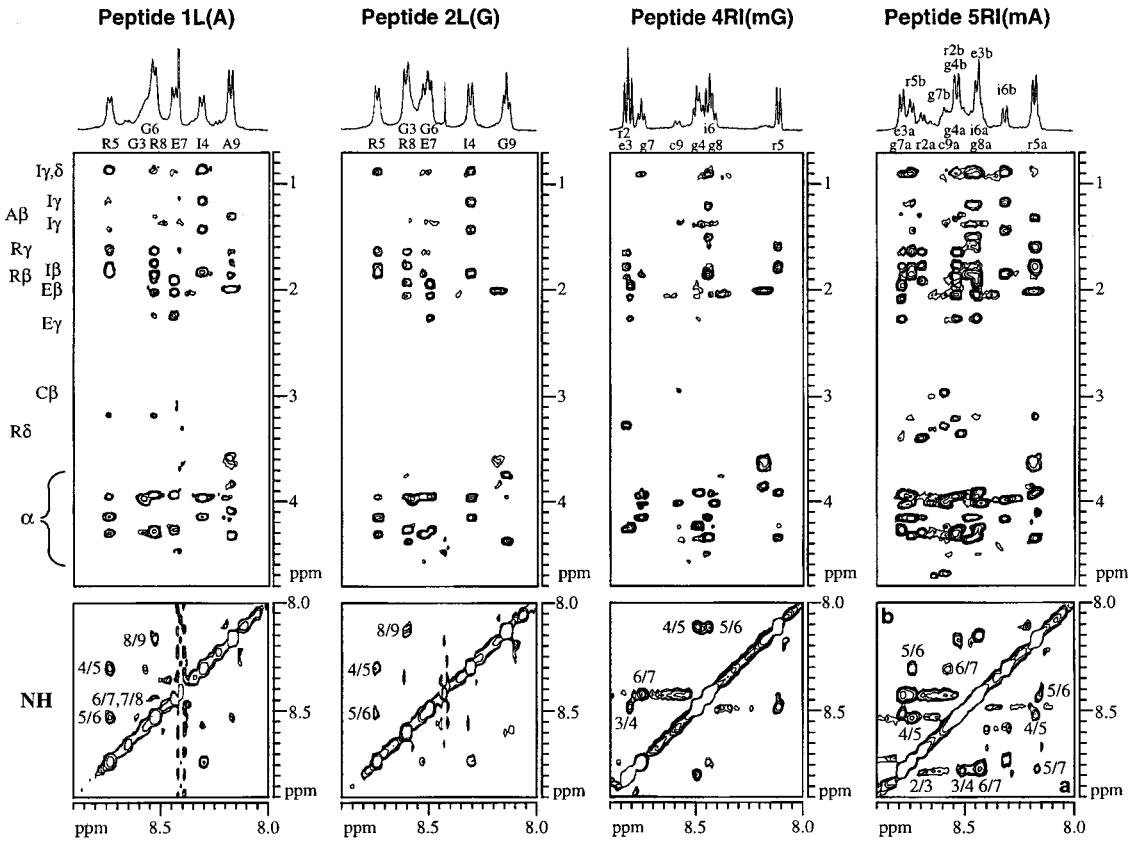

FIGURE 1: CH−NH (top) and NH−NH (bottom) correlations in the TR-NOESY spectra for the L(A) and L(G) parent peptides and for the RI(mG) and RI(mA) retro−inverso peptides in the presence of 2% mAb 4x11 antibody in H_2O and D_2O (95/5, v/v) (pH 7.0 and 4 °C, mixing time = 200 ms). The water signal is suppressed with the WATERGATE sequence using field gradient pulses. Distinction between the two diastereoisomers [RIa(mA) and RIb(mA)] is delineated by the separated sequential assignment of the NN(i,i+1) TR-NOE cross-peaks.

appreciated by considering the difference between the amide chemical shifts, which are very sensitive to the environment, in the homologous positions (Figure 2), although the amide chemical shifts represent only an average value over many folded and unfolded conformations in water. The two parent peptides L(A) and L(G) only exhibit very small differences (Figure 2a), and the same is true for L(A) and L(a) except for the modified C-terminal residue (Figure 2b). This observation seems to indicate that all three peptides have quite similar conformational properties. As already mentioned, the retro−inverso peptides RI(mG) and RIa(mA) exhibit quite similar NH resonance frequencies (Figure 2f) and therefore exhibit the same NH perturbation profile compared with the parent peptide L(A), with opposed perturbations for the residues in positions G3 or G7, I4 or i6, E7 or e3, and R8 or r2 on one hand, and for arginine in position 5 on the other hand (Figure 2c,d). It is surprising that, at variance with RIa(mA) and RI(mG), the distribution of the amide proton resonances for the RIb(mA) isomer is identical to that for the parent peptide L(A) (Figure 2e). Since δ_{NH} is sensitive to the NH environment, it is suggesting that RIb(mA) and L(A) have a similar chemical environment. We therefore may infer that the diastereomers RIa(mA) and RIb(mA), which only differ in the chirality of the terminal malonic residue, have quite different conformational behaviors.

The NH−NH and CH−NH NOESY correlations at τ_m = 200 ms (Figure 1) illustrate weak to intense sequential αN(i,i+1) and medium to intense intraresidue αN(i,i), βN(i,i), and γN(i,i) TR-NOEs. Other $\alpha\beta(i,i)$, $\beta\gamma(i,i)$, and $\gamma\delta(i,i)$ intraresidue TR-NOEs (not shown) probably reflect a constrained orientation of most of the side chains in the complex. In Figure 3 is shown for the mAb-bound antigens the conventional representation for the NOE connectivities, classified according to their relative intensities. Most of the NN(i,i+1) connectivities are visible in every four cases, but the absence of consecutive strong NN(i,i+1) and αN(i,i+1) TR-NOEs, and of weak consecutive $\alpha\beta(i,i+3)$ and αN(i,i+3) TR-NOEs, allows us to exclude any helical or β-strand structure (*44*). The simultaneous occurrence of intense NN(I4,R5), strong αN(G3,I4), and weak αN(G3,R5) TR-NOEs for both L(A) and L(G) indicates a β-turn (G2G3I4R5 sequence) in the L-peptides. Similarly, the strong NN(G4,r5) and weak NN(e3,r5) TR-NOEs for both retro−inverso peptides RI(mG) and RIa(mA) are typical of a β-turn (r2e3G4r5 sequence). Due to partial overlapping of the NH signals for the RI(mA) diastereomers, and also to its probable weaker mAb affinity, only very few TR-NOEs could be quantified for RIb(mA).

Three-Dimensional Structure. Molecular calculations on L(A), L(G), RIa(mA), and RI(mG) came up against two main difficulties: (i) the CG terminus of the flexible CGG extension as a linker to the dextran matrix in BIAcore experiments is not tightly recognized by the antibody and gives rise to a small number of very weak TR-NOEs, and (ii) the Gly $C^{\alpha}H_2$ protons have not been stereospecifically

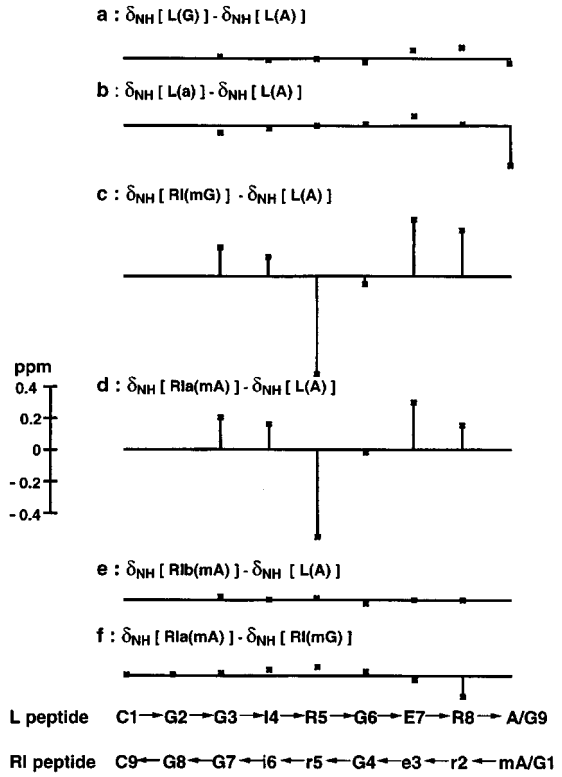

FIGURE 2: Perturbations of the amide proton resonances for selected derivatives with reference to the parent peptide L(A) (a−e) or to the retro−inverso peptide RI(mG) (f).

assigned even when they are magnetically nonequivalent [G7 $C^{\alpha}H_2$ of RI(mG) and RIa(mA)] (the same holds true for the $C^{\beta}H_2$ group). In these cases, a pseudoatom was created with a reduced force constant to take the corresponding NOEs into account. When we started from the extented structure, 50 structures were extracted from a 200 ps duration of restrained MD at 1000 K and submitted to a cooling SA protocol (*43*) as outlined in Materials and Methods. About half of them for which the ϕ dihedral angles adopt negative values for the L-residues and positive values for the D-residues have been retained. Due to the small number of TR-NOEs collected for the RIb(mA) stereomer, molecular simulation has not been performed in this case. The set of TR-NOE distance restraints for RIa(mA) has been independently applied to both stereomers containing the (*R*)- or (*S*)-2-methylmalonic acid residue. Figure 4 is a superposition of the eight modeled structures with minimum energy for the five investigated derivatives. The central part of each peptide has a rather rigid conformation, whereas both N- and C-termini are much more flexible, in agreement with the small number of TR-NOEs collected for these regions. In Table 1 are listed the ϕ, ψ, and χ_1 values (with their standard deviation) for the averaged structures calculated from the structures retained for the SA process. The increased or decreased flexibility of the segments may be appreciated from the magnitude of the estimated standard deviations.

L-Parent Peptide. The ϕ and ψ dihedral angles defining the turn in the G2G3I4R5 sequence (Table 1) closely fit the consensus values of 60° and −130° for ϕ and ψ, respectively, and −90° and 0° for ϕ and ψ, respectively, typical for the type II′ β-turn. In agreement with their quite similar NH resonances (Figure 2a), the L(A) and L(G) peptides have

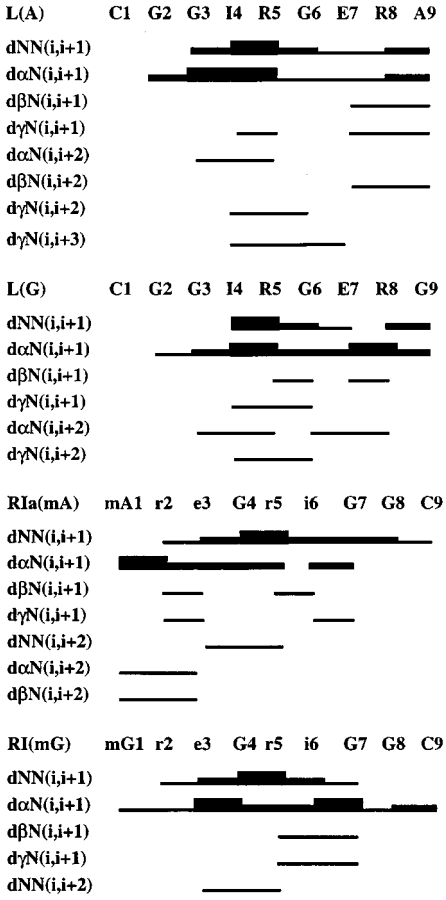

FIGURE 3: Schematic $^1H-^1H$ TR-NOE connectivities for the L(A) and L(G) parent peptides and for the RI(mG) and RIa(mA) retro−inverso peptides in the presence of 2% mAb 4x11 antibody in H_2O and D_2O (95/5, v/v). The TR-NOE intensities are classified as strong, medium, or weak and represented by lines with decreasing thicknesses.

practically the same conformational properties in the mAb-bound state and appear to be composed of the rather rigid βII′-folded G2G3I4R5 and extended G6E7R8A/G9 sequences, while the G2 and G6 residues allow a local flexibility. Pairwise superimposition of the G2G3I4R5 backbone atoms for the three-dimensional structures having the lowest energy after SA calculations corresponds to rmsd values of 0.6 and 0.7 Å for the L(A) and L(G) peptides, respectively. Similarly, pairwise superimposition of the extended G6E7R8A/G9 backbone atoms results in rmsd values of 0.7 Å for L(A) and L(G).

Retro−Inverso Peptides. Only RI(mG) and the RIa(mA) diastereomer gave significant and numerous TR-NOEs that could be used for MD simulations. The ϕ and ψ dihedral angles defining the turn in the r2e3G4r5 sequence (Table 1) are in favor of the type I′ β-turn having the consensus values of 60° and 30° for ϕ and ψ, respectively, and 90° and 0° for ϕ and ψ, respectively. In the absence of configurational assignment of the terminal 2-methylmalonic acid residue, the TR-NOEs for RIa(mA) have been applied to both diastereomers containing either the (*R*)- or (*S*)-2-methylmalonic acid residue. Pairwise superimposition of the r2e3G4r5i6 backbone atoms for the three-dimensional structures having the lowest energy after SA calculations (Figure 4) corresponds to an rmsd value of 0.3 Å for both RI(m*R*-A) and RI(mG), and 0.5 Å for RI(m*S*-A). The RI(mG) conformation

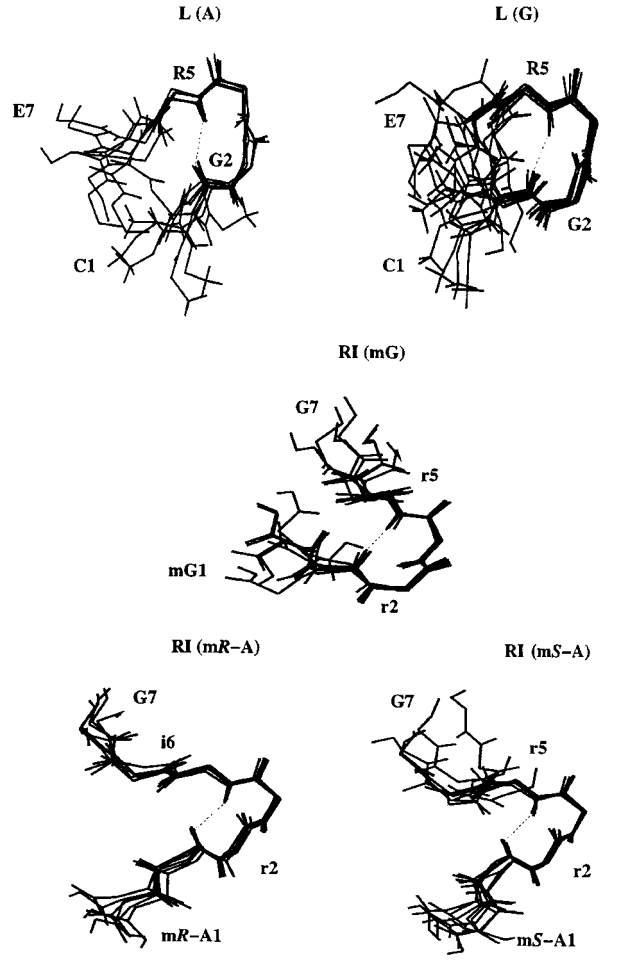

FIGURE 4: Superposition of the CGGIRGE and eGriGGC sequences of the eight lowest-energy structures for the mAb-bound IRGERA L- and retro−inverso nonapeptides, issued from simulated annealing and restrained MD calculations. All structures are superimposed on the GGIR and riGG sequences having the lowest-energy structure by least-squares fitting of the backbone atoms.

partly fits those for RI(m*R*-A) and RI(m*S*-A), but gives a smaller rmsd for RI(m*R*-A) (0.5 Å) than for RI(m*S*-A) (1.0 Å). In addition, the SA simulations show a larger disorder for the N-terminal mA residue when calculations were performed with the *S*-enantiomer (standard deviation equals 112° for the ψ torsion angle value instead of 5° observed in the case of the *R*-configuration) (Table 1). This result suggests that the RIa(mA) stereomer, having the higher mAb affinity, probably contains the (*R*)-2-methylmalonic acid residue which leads to fewer restraint violations and has the same absolute chirality as the D-Ala residue in a retro−inverso peptide. The stereomer RIb(mA) with weaker mAb affinity is thus assigned to RI(m*S*-A). RI(mG) and RI(m*R*-A) exhibit quite similar conformational properties.

DISCUSSION

According to the results obtained by the ELISA, mAb generated against the L-peptide cross reacted equally well with the L- and RI peptides. In contrast, BIAcore measurements showed that the affinity constant K_a of the mAb was 75-fold higher with RI(mA) than with the homologous L(A) peptide (*13*, *34*). The lack of direct correlation between OD values in ELISA and the K_a values measured in the BIAcore instrument may be due to the low diffusion rate in microtiter wells, leading to fast antibody reassociation and very low apparent rates of dissociation (*12*, *49*, *50*). The different microenvironments of the peptides either in the dextran layer of the sensor chip or as BSA conjugates coated on the plastic surface of the ELISA plate might also be responsible for the observed differences. In the BIAcore system, the peptide is immobilized on the sensor chip while the antibody preparation is injected at a constant flow rate over the course of 7 min. The equilibrium affinity constants determined in these conditions can be very different from those measured in the TR-NOE experiments when the ligand is in solution and in a large excess with reference to the mAb. The K_D values measured in the BIAcore instrument are around $10^{-7}-10^{-9}$ M. The binding affinity constants measured by TR-NOESY and in the BIAcore system thus differ by ~3−5 orders of magnitude. The NMR and BIAcore binding affinity measurement scales are not quantitatively comparable. According to the BIAcore affinity magnitudes, no signal should be observed in TR-NOESY experiments. It is notable, on the other hand, that no TR-NOE effect was observed for the D-Ala9 analogue, which is not recognized by the mAb. The fact that the TR-NOE effects observed for the other antigens are the result of some secondary weak binding site thus has to be discarded. Despite the discrepancy between the NMR and BIAcore results, the conformational results, as issued from our NMR and MD simulation, are qualitatively coherent and consistent with ELISA and BIAcore results.

The antibody-bound structure determination by SA simulations from TR-NOESY experiments reveals that the folding modes of the L- and retro−inverso peptide antigens are quite different. The L-peptides exhibit two regions with a defined structure: a βII′-folded GGIR sequence and an extended GERA sequence, connected by a glycine residue allowing a local flexibility. It is remarkable that the βII′-turn involves the CGG extension introduced as a linker into the liposomes, or into the sensor chip in BIAcore experiments. On the contrary, the retro−inverso peptides exhibit a βI′-folded reGr sequence, topologically equivalent to a βI-folded sequence in the homologous L-peptide, which is located in the central part of the antigenic sequence. Among the different structures assumed by antibody-bound peptides, the β-turn is an important structural motif for antibody recognition (*51*, *52*). We may infer that, in the BIAcore experiments, the turn in the L-peptide antigens is close to the dextran chip, and therefore probably less accessible to the circulating antibody than the turn in the retro−inverso analogues. Furthermore, the turn in the retro−inverso peptides is an intrinsic property of the antigenic sequence, whereas that in the L-peptides depends on the nature of the linker. In histone H3, the IRGERA sequence is preceded by ARR, and the chirality of RRIR is probably not compatible with the type II′ β-turn assumed by GGIR (*53*). The fact that the same antibody is capable of recognizing different conformations illustrates the flexibility of the antibody in induced fit antigen−antibody association. However, we have no experimental information about the respective disposition of the L-peptide or retro−inverso peptide and the antibody binding site.

In a previous study on antibodies raised against histone H3 or the IRGERA peptide, it was noted that the substitution of the D-enantiomer for either E7, R8, or A9 drastically altered the antigenicity of the modified resulting analogues.

Table 1: Averaged ϕ, ψ, and χ_1 Values (Degrees) of All the Retained SA Structures for the L- and RI Nonapeptides in the Presence of the mAb 4x11 Antibody

residue	torsion angle	L(A)	L(G)	RI(mG)	RI(m*R*-A)	RI(m*S*-A)
C1 or C9	ϕ			113 ± 64	100 ± 62	126 ± 31
	ψ	117 ± 73	116 ± 52			
	χ_1	168 ± 82	−99 ± 76	178 ± 46	161 ± 92	168 ± 91
G2 or G8	ϕ	−174 ± 81	−172 ± 28	173 ± 13	−133 ± 92	−164 ± 77
	ψ	−56 ± 95	−148 ± 73	52 ± 101	106 ± 104	115 ± 84
G3 or G7	ϕ	69 ± 10	74 ± 10	−87 ± 72	−127 ± 78	−162 ± 64
	ψ	−130 ± 30	−101 ± 17	21 ± 32	−69 ± 105	−70 ± 103
I4 or i6	ϕ	−90 ± 32	−97 ± 32	91 ± 13	99 ± 34	92 ± 22
	ψ	6 ± 23	−3 ± 17	44 ± 70	−12 ± 67	−19 ± 60
	χ_1	105 ± 78	175 ± 94	79 ± 77	−88 ± 95	55 ± 99
R5 or r5	ϕ	−157 ± 5	−154 ± 4	145 ± 5	135 ± 8	129 ± 20
	ψ	154 ± 78	101 ± 57	−91 ± 8	−86 ± 3	−70 ± 60
	χ_1	−172 ± 66	−130 ± 89	152 ± 80	123 ± 57	137 ± 56
G6 or G4	ϕ	−117 ± 38	151 ± 86	81 ± 4	82 ± 3	79 ± 7
	ψ	77 ± 16	157 ± 73	18 ± 7	18 ± 5	15 ± 9
E7 or e3	ϕ	−159 ± 2	−157 ± 2	50 ± 5	51 ± 2	53 ± 4
	ψ	132 ± 83	115 ± 92	42 ± 4	41 ± 4	41 ± 4
	χ_1	164 ± 65	−171 ± 52	153 ± 95	−105 ± 99	113 ± 105
R8 or r2	ϕ	−158 ± 4	−156 ± 3	86 ± 31	105 ± 15	96 ± 6
	ψ	95 ± 70	94 ± 51	72 ± 34	−93 ± 6	−74 ± 14
	χ_1	130 ± 93	−149 ± 46	123 ± 55	96 ± 58	166 ± 89
A9 or G9/mA1 or mG1	ϕ	−178 ± 69	175 ± 68			
	ψ				−110 ± 5	−71 ± 112
	χ_1	164 ± 82			117 ± 65	63 ± 91

Therefore, the C-terminal E7, R8, and A9 residues are strictly required for mAb recognition. On the contrary, replacement of R5 with L-lysine or D-alanine was found to change neither the antigenic nor immunogenic properties of the resulting peptides (*34*). Pairwise superimposition of the extended G6E7R8A9 backbone atoms in L(A) for the three-dimensional structure having the lowest energy after SA calculations with those of the G4e3r2m*R*-A1 sequence in RI(m*R*-A) shows that the side chains for each couple of the three essential E7 or e3, R8 or r2, and A9 or m*R*-A1 residues are similarly orientated with respect to the backbone (Figure 5). Figure 5 also shows that the Glu and Arg side chains are less flexible in RI(m*R*-A) than in the L(A) parent peptide, a feature which is probably related to the fact that RI(m*R*-A) is significantly tightly recognized compared to the L-peptide by the antibody. This observation, together with the fact that the antigen−antibody interaction accommodates an inversion of the amide link, would suggest that the side chains of the antigen are more directly involved in the mAb contact than the peptide backbone atoms.

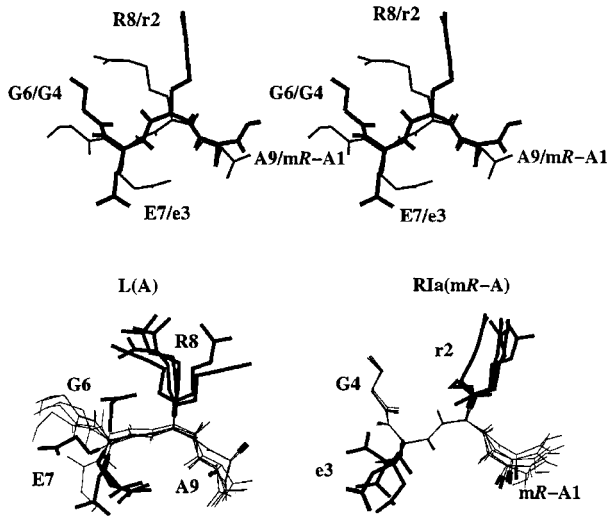

FIGURE 5: Comparison between the best lowest SA three-dimensional structure of the GERA sequence of the L-peptide with that of the Germ*R*-A sequence of the retro−inverso peptide. Stereoview showing that the side chain of a given residue (E7 or e3, R8 or r2, and A9 or m*R*-A1) is pointing to the same direction when comparing the mAb-bound structure of L(A) and RI(m*R*-A) (top). Because the peptide bonds were inverted, only the C^{α} atoms were taken into consideration for superposition. Superposition of six lowest-energy structures for the G6−A9 sequence in L(A) and the m*R*-A1−G4 sequence in RIa(m*R*-A) (bottom). For both stereoviews, the backbone skeleton is depicted with thin lines and side chains are depicted with thick lines.

FINAL COMMENTS

In this study, we have shown that the β-turn behaves as a secondary structural template allowing adequate presentation of the essential side chains to the antibody binding site. Indeed, the L- and retro−inverso IRGERA peptides, recognized by the same monoclonal antibody, form two distinct β-turns of different types, which involve two distinct regions of the antigenic peptides. The L-peptides do present a type II′ β-turn at the N-terminus, but this region contains the CGG linker and could be not essential to antibody recognition in this case. On the contrary, the folded type I′ β-turn in the retro−inverso analogue concerns the four central epitope residues, and the equilibrium affinity constant K_a measured for the RI(mG) analogue approaches that for the intact histone H3. The retro−inverso peptides are thus able to mimic favorably the antigenic site in the complete protein.

On the other hand, SA simulations have shown that the side chain for each of the three essential Glu7 (glu3), Arg8 (arg2), and Ala9 (m*R*-Ala1) residues has the same orientation in both the L- and retro−inverso peptides with respect to the backbone. This observation could explain why the retro−inverso peptides are more tightly recognized than their respective parent L-peptides. Finally, SA simulations suggest that the (*R*)-2-methylmalonic acid that mimics the D-Ala N-terminal residue should be assigned to RIa(mA) which is the diastereomer having the highest K_a value.

ACKNOWLEDGMENT

Access to the Bruker DRX 400 NMR facilities of the Service Commun de Résonance Magnétique Nucléaire of the Université Henri Poincaré, Nancy I, was deeply appreciated. We thank Dr. Michel Marraud and Dr. Johan Hoebeke for many valuable suggestions and critical comments, Dr. Nadia Benkirane for skilful help with affinity measurements, and Mr. Jean-Marie Grosse for computer assistance.

REFERENCES

1. Fauchère, J.-L., and Thurieau, C. (1992) *Adv. Drug Res. 23*, 128−154.
2. Giannis, A., and Kolter, T. (1993) *Angew. Chem., Int. Ed. 32*, 1244−1267.
3. Gante, J. (1994) *Angew. Chem., Int. Ed. 33*, 1699−1720.
4. Qabar, M., Urban, J., Sia, C., Klein, M., and Kahn, M. (1996) *Il Farmaco 51*, 87−96.
5. Shemyakin, M. M., Ovchinnikov, Y. U., and Ivanov, V. T. (1969) *Angew. Chem., Int. Ed. 8*, 492−499.
6. Hruby, V. J., Al-Obeidi, F., and Kazmierski, W. (1990) *Biochem. J. 268*, 249−262.
7. Marraud, M., Dupont, V., Grand, V., Zerkout, S., Lecoq, A., Boussard, G., Vidal, J., Collet, A., and Aubry, A. (1993) *Biopolymers 33*, 1135−1148.
8. Chorev, M., and Goodman, M. (1993) *Acc. Chem. Res. 26*, 266−273.
9. Leban, J. J., Kull, F. C., Jr., Landavazo, A., Stockstill, B., and McDermed, J. D. (1993) *Proc. Natl. Acad. Sci. U.S.A. 90*, 1922−1926.
10. Merrifield, R. B., Juvvadi, P., Andreu, D., Ubach, J., Boman, A., and Boman, H. G. (1995) *Proc. Natl. Acad. Sci. U.S.A. 92*, 3449−3453.
11. Fletcher, M. D., and Campbell, M. M. (1998) *Chem. Rev. 98*, 763−795.
12. Guichard, G., Benkirane, N., Zeder-Lutz, G., Van Regenmortel, M. H. V., Briand, J. P., and Muller, S. (1994) *Proc. Natl. Acad. Sci. U.S.A. 91*, 9765−9769.
13. Benkirane, N., Guichard, G., Van Regenmortel, M. H. V., Briand, J.-P., and Muller, S. (1995) *J. Biol. Chem. 270*, 11921−11926.
14. Muller, S., Guichard, G., Benkirane, N., Brown, F., Van Regenmortel, M. H. V., and Briand, J. P. (1995) *Pept. Res. 8*, 138−144.
15. Briand, J. P., Benkirane, N., Guichard, G., Newman, J. F. E., Van Regenmortel, M. H. V., Brown, F., and Muller, S. (1997) *Proc. Natl. Acad. Sci. U.S.A. 94*, 12545−12550.
16. Nargi, F., Kramer, E., Mezencio, J., Zamparo, J., Whetstone, C., Van Regenmortel, M. H. V., Briand, J. P., Muller, S., and Brown, F. (1999) *Vaccine 17*, 2888−2893.
17. Briand, J.-P., Guichard, G., Dumortier, H., and Muller, S. (1995) *J. Biol. Chem. 270*, 20686−20691.
18. McDonnell, J. M., Beavil, A. J., Mackay, G. A., Jameson, B. A., Korngold, R., Gould, H. J., and Sutton, B. J. (1996) *Nat. Struct. Biol. 3*, 419−426.
19. Ostankovitch, M., Guichard, G., Connan, F., Muller, S., Chaboissier, A., Hoebeke, J., Choppin, J., Briand, J.-P., and Guillet, J. G. (1998) *J. Immunol. 161*, 200−208.
20. Okamoto, S., Watanabe, M., Yamazahi, M., Yajima, T., Hayashi, T., Ishii, H., Mukai, M., Yamada, T., Watanabe, N., Jameson, B. A., and Hibi, T. (1999) *Eur. J. Immunol. 29*, 355−366.
21. Petit, M. C., Benkirane, N., Guichard, G., Phan-Chan-Du, A., Marraud, M., Cung, M. T., Briand, J.-P., and Muller, S. (1999) *J. Biol. Chem. 274*, 3686−3692.
22. Clore, G. M., and Gronenborn, A. M. (1982) *J. Magn. Reson. 48*, 402−417.
23. Yamazaki, T., Mierke, D. F., Said-Nejad, O. E., Felder, E. R., and Goodman, M. (1992) *Int. J. Pept. Protein Res. 39*, 161−181.
24. Carver, J. A., Esposito, G., Viglino, P., Fogolari, F., Guichard, G., Briand, J.-P., Van Regenmortel, M. H. V., Brown, F., and Mascagni, P. (1997) *Biopolymers 41*, 569−590.
25. Higgins, K. A., Bicknell, W., Keah, H. H., and Hearn, M. T. W. (1997) *J. Pept. Res. 50*, 421−435.
26. McDonnell, J. M., Fushman, D., Cahill, S. M., Sutton, B. J., and Cowburn, D. (1997) *J. Am. Chem. Soc. 119*, 5321−5328.
27. Otting, G. (1993) *Curr. Opin. Struct. Biol. 3*, 760−768.
28. Campbell, A. P., and Sykes, B. D. (1993) *Annu. Rev. Biophys. Biomol. Struct. 22*, 99−122.
29. Anglister, J., and Naider, F. (1991) *Methods Enzymol. 203*, 228−241.
30. Rosevear, P. R., and Mildvan, A. S. (1989) *Methods Enzymol. 117*, 333−375.
31. Neimark, J., and Briand, J. P. (1993) *Pept. Res. 6*, 219−228.
32. Chorev, M., Rubini, E., Gilon, C., Wormser, U., and Selinger, Z. (1983) *J. Med. Chem. 26*, 129−135.
33. Zeder-Lutz, G., Altschuh, D., Denery-Papini, S., Briand, J.-P., Tribbick, G., and Van Regenmortel, M. H. V. (1993) *J. Mol. Recognit. 6*, 71−79.
34. Benkirane, N., Friede, M., Guichard, G., Briand, J.-P., Van Regenmortel, M. H. V., and Muller, S. (1993) *J. Biol. Chem. 268*, 26279−26285.
35. Kumar, A., Wagner, G., Ernst, R. R., and Wuthrich, K. (1981) *J. Am. Chem. Soc. 103*, 3654−3658.
36. Cung, M. T., Demange, P., Marraud, M., Tsikaris, V., Sakarellos, C., Papadouli, I., Kokla, A., and Tzartos, S. J. (1991) *Biopolymers 31*, 769−776.
37. Piotto, M., Saudek, V., and Sklenar, V. (1992) *J. Biomol. NMR 2*, 661−666.
38. Bartels, C., Xia, T.-H., Billeter, M., Güntert, P., and Wüthrich, K. (1995) *J. Biomol. NMR 5*, 1−10.
39. Güntert, P., Mumenthaler, C., and Wüthrich, K. (1997) *J. Mol. Biol. 273*, 283−298.
40. Dauber-Osguthorpe, P., Roberts, V. A., Osguthorpe, D. J., Wolff, J., Genest, M., and Hagler, A. T. (1988) *Proteins: Struct., Funct., Genet. 4*, 31−47.
41. Clore, G. M., and Gronenborn, A. M. (1987) *Protein Eng. 1*, 275−288.
42. Koradi, R., Billeter, M., and Wüthrich, K. (1996) *J. Mol. Graphics 14*, 51−55.
43. Nilges, M., Clore, G. M., and Gronenborn, A. M. (1988) *FEBS Lett. 229*, 317−324.
44. Clore, G. M., Brunger, A. T., Karplus, M., and Gronenborn, A. M. (1986) *J. Mol. Biol. 191*, 523−551.
45. Scheek, R. M., van Gusteren, W. F., and Kaptein, R. (1989) *Methods Enzymol. 177*, 204−218.
46. Campbell, A. P., and Sykes, B. D. (1991) *J. Magn. Reson. 93*, 77−92.
47. Campbell, A. P., and Sykes, B. D. (1991) *J. Biomol. NMR 1*, 391−402.
48. Wüthrich, K. (1986) *NMR of Proteins and Nucleic Acids*, pp 162−166, Wiley, New York.
49. Sternberg, M., and Nygren, H. (1988*) J. Immunol. Methods 113*, 3−15.
50. Azimzadeh, A., Pellequer, J. L., and Van Regenmortel, M. H. V. (1992) *J. Mol. Recognit. 5*, 9−18.
51. Wilson, I. A., and Stanfield, R. L. (1994) *Curr. Opin. Struct. Biol. 4*, 857−867.
52. Kuntz, I. D. (1972) *J. Am. Chem. Soc. 94*, 4009−4012.
53. Rose, G. D., Gierasch, L. M., and Smith, J. A. (1985) *Adv. Protein Chem. 37*, 1−109.

BI001151H